Hindawi
Journal of Nanomaterials
Volume 2019, Article ID 9486745, 9 pages
https://doi.org/10.1155/2019/9486745

Research Article

Structural Evolution and Photoluminescence of SiO_2 Layers with Sn Nanoclusters Formed by Ion Implantation

I. Romanov,[1] F. Komarov,[2] O. Milchanin,[2] L. Vlasukova,[1] I. Parkhomenko,[1] M. Makhavikou,[2] E. Wendler,[3] A. Mudryi,[4] and A. Togambayeva[5]

[1]*Belarusian State University, 4 Nezavisimosti Ave, Minsk 220030, Belarus*
[2]*A.N. Sevchenko Research Institute of Applied Physical Problems, Belarusian State University, 7 Kurchatova St., Minsk 220045, Belarus*
[3]*Institut für Festkörperphysik, Friedrich-Schiller-Universität Jena, Max-Wien-Platz 1, D-07743 Jena, Germany*
[4]*Scientific and Practical Materials Research Center, National Academy of Sciences of Belarus, P. Brovki Str. 17, 220072 Minsk, Belarus*
[5]*Al-Farabi Kazakh National University, Al-Farabi Ave. 71, Almaty 050040, Kazakhstan*

Correspondence should be addressed to F. Komarov; komarovf@bsu.by

Received 18 July 2018; Revised 28 November 2018; Accepted 9 December 2018; Published 26 March 2019

Guest Editor: Bathula Babu

Samples of SiO_2 (600 nm)/Si have been implanted with Sn ions (200 keV, 5×10^{16} cm^{-2} and 1×10^{17} cm^{-2}) at room temperature and afterwards annealed at 800 and 900°C for 60 minutes in ambient air. The structural and light emission properties of "SiO_2 +Sn-based nanocluster" composites have been studied using Rutherford backscattering spectroscopy, transmission electron microscopy in cross section and plan-view geometry, electron microdiffraction, and photoluminescence (PL). A strict correspondence of Sn concentration profiles and depth particle distributions has been found. In the case of 1×10^{17} cm^{-2} fluence, the impurity accumulation in the subsurface zone during the thermal treatment leads to swelling and to the formation of dendrites composed of large and coalesced nanoparticles of grey contrast. The appearance of dendrites is most probably due to the SnO_2 phase formation. The as-implanted samples are characterized by a weak emission with maximum at the blue range (2.9 eV). The PL intensity increases by an order of magnitude after annealing in an oxidizing atmosphere. The narrowest and most intense PL band has maximum at 3.1 eV. Its intensity increases with increasing fluence and annealing temperature. This emission can be attributed to the formation of the SnO_2 phase (in the form of separate clusters or shells of Sn clusters) in the subsurface region of the SiO_2 matrix.

1. Introduction

Silicon dioxide layers are the most common material in optical fiber manufacturing and microelectronics as a thin electric isolator in a metal-oxide-semiconductor (MOS) transistor and a diffusion barrier. At present, adding optical functionality to a silicon microelectronic chip is one of the most challenging problems of materials research. Thereby, considerable efforts have been focused on the enhancement of UV and visible emission from silica to create an active light-emitting element in next-generation miniature optoelectronic devices [1–12]. In spite of typical optoelectronic's operation in IR range, the creation of such silica-based emitters operating in both the visible and UV-violet spectral ranges is a perspective for creating a microminiature MOS light-emitting diode (LED), Bragg reflectors, waveguide lasers, and optocouplers as well as optical switchers in color microdisplay devices. To fabricate a low-cost effective silica-based LED, the ion implantation approach seems quite promising because of well-controlled impurity atom distribution and/or impurity-based nanocrystal formation, good passivation from ambient condition, and excellent compatibility with Si MOS processes [1–4, 10–12].

It is reported that Si-, Ge-, and Sn-implanted SiO_2 films exhibit strong blue-violet (UV) photoluminescence (PL) [1–4]. According to Ref. [1], the Sn-rich silica films exhibit

the strongest photoluminescence (PL) intensity among these composites. Motivated by this result, we devote the present article to Sn-implanted silicon oxide films.

Although the modification of the SiO_2 matrix by means of ion implantation for a light emission increase is developed sufficiently, the unsolved problems still remain. Among them, the main one is a mechanism of radiative recombination. On the one hand, ion implantation results in modification of the silica matrix. So, high-fluence Sn implantation results in the formation of optical active oxygen divacancies (twofold coordinated Sn atom bonded to the rest of the silica network via two oxygen atoms). Such Sn-related color centers emit PL at 3.15 eV due to a triplet-singlet transition [1, 5, 13]. On the other hand, high-fluence ion implantation results in the formation of nanoclusters in the silica matrix. Namely, Sn implantation followed by heat treatment can result in the formation of different Sn-based phases depending on the annealing regime and environment. Namely, the formation of metallic β-Sn precipitates as well as SnO_x nanoparticles can take place after annealing in vacuum or N_2 ambient condition in the range of 600–1100°C [3, 4]. In some cases, Sn cores with SnO_{2-x} shells were found [3]. On the contrary, the formation of SnO_2 nanoparticles also took place after annealing in an oxidizing atmosphere (air or pure oxygen) in the temperature range of 400–1000°C [10, 11, 14]. Tin dioxide is known as a semiconductor with a wide direct bandgap of 3.6 eV, which is dipole forbidden. But direct gap luminescence can be allowed in SnO_2 nanocrystals (NCs). Indeed, nanocrystalline SnO_2 thin films [15, 16] and nanoparticles [17] exhibit strong UV and visible luminescence, which is dependent on surface states and deep-level defects. Thus, it is important to clarify what processes (modification of the silica matrix itself or creation of a new phase in the form of nanoclusters) play a crucial role in a radiative recombination mechanism in Sn-implanted silica.

Considering the complicated phase composition as well as the presence of different radiative and nonradiative centers in Sn-implanted films, the deep analysis of structural and luminescence properties depending on the regime of implantation and subsequent annealing is needed. In spite of a number of publications devoted to silicon oxide films implanted with Sn ions [1–4, 10–12], the influence of implantation fluence on their structure and luminescence was studied insufficiently. In this paper, we report the structural and light-emitting properties of "SiO_2+Sn-based NC" composites created by means of Sn^+ implantation with two different fluences into SiO_2 on Si followed by oxidation in ambient air. We have tried to find out a correlation between Sn concentration depth profiles, Sn-based precipitate distributions in the SiO_2 layers, and photoluminescence of composites under investigation.

2. Experiment

The initial samples (2×2 cm^2) of SiO_2/Si structures were cut from the thermally oxidized Si substrates. The thickness of the SiO_2 layer as measured by transmission electron microscopy in cross section geometry (XTEM) was 600 nm. These samples were implanted at room temperature with 200 keV Sn ions to fluences of 5×10^{16} and 1×10^{17} cm^{-2}. Computer simulation (SRIM) gave Gaussian-type Sn concentration-depth profiles with the peak concentrations of about 11 at.% (for 5×10^{16} cm^{-2}) and of about 22 at.% (for 1×10^{17} cm^{-2}) formed at the depth of 100 nm in the oxide matrix. Afterwards, a part of the samples was annealed at 800 or 900°C for 60 min in ambient air.

The Sn distribution profiles of the implanted and annealed samples were analyzed by Rutherford backscattering spectroscopy (RBS), using 1.5 MeV He^+ ions. Fitting of experimental RBS spectra to the simulated ones was carried out using the SIMNRA code. In the calculated concentration profiles of tin atoms, the transition of the depth scale from the laboratory coordinate system to the metric one was carried out on the basis of the thickness of the oxide layer of the samples measured by transmission electron microscopy (TEM).

The structural investigations and phase analysis in the samples were carried out using TEM in "plan-view" and "cross section" geometry as well as electron microdiffraction. A Hitachi H-800 analytical electron microscope operating at 200 keV was used for these studies. Samples for TEM research in both geometries ("plan-view" and "cross-section") were prepared by the conventional technique that included precision cutting, cutting wheels, grinding, polishing, and Ar^+ ion polishing using Gatan equipment. In the finishing treatment, low energies of ion beams (3-5 keV) and sliding etching angles (3-5°) were used, which ensured the nonintroduction of structural defects into the samples during their preparation.

Photoluminescence spectra were recorded at room temperature in the energy range of 1.77–3.54 eV using a diffraction monochromator with a focal distance of 0.6 m. The 3.81 eV (325 nm) emission line of a continuous wave He-Cd laser was used for excitation. The emission bandwidth of equipment was chosen to be 1 nm. Additionally, PL excitation (PLE) spectra were registered.

One of the samples implanted to the fluence of 1×10^{17} cm^{-2} and annealed at 900°C was additionally treated in a 4% hydrofluoric acid (HF) aqueous solution at room temperature. A part of this sample was protected during the chemical treatment. The thickness of the etched layer was estimated via the comparison of the SiO_2 film color between the protected and unprotected regions of the etched sample. It is known that slight changes in the thickness of dielectric films create major shifts in their perceived color. One can estimate the thickness of the film simply by observing its color and comparing it with color charts (see, for example, Ref. [18]). In the case of SiO_2 films, a thickness variation of about 50 nm can be noticed via its color change [19].

3. Results and Discussion

3.1. Composition and Structure of "SiO_2+Sn-Based NC" Composites. Figures 1–3 display the cross-sectional TEM images of the Sn nanocluster distribution in as-implanted and annealed samples. The solid white lines in the right side of every TEM image give the depth distribution of Sn atoms as detected by RBS spectral simulations.

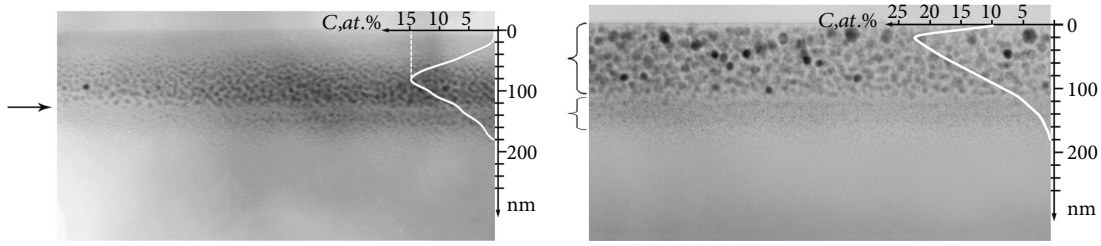

(a) (b)

FIGURE 1: XTEM images of SiO_2 (600 nm)/Si samples implanted with 200 keV Sn^+ to a fluence of 5×10^{16} cm^{-2} (a) and 1×10^{17} cm^{-2} (b). In the right of each XTEM image, the depth distribution of Sn (given in at.%) is shown as detected by RBS.

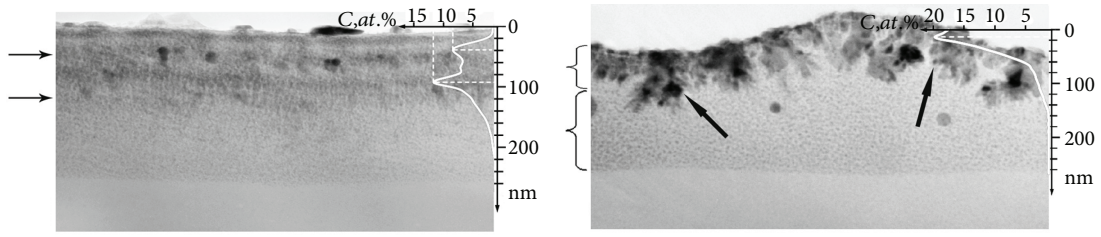

(a) (b)

FIGURE 2: XTEM images of SiO_2 (600 nm)/Si samples implanted with 200 keV Sn^+ to a fluence of 5×10^{16} cm^{-2} (a) and 1×10^{17} cm^{-2} (b) and annealed for 60 minutes at 800°C. In the right of each XTEM image, the depth distribution of Sn (given in at.%) is shown as detected by RBS. The arrows in (a) and braces in (b) are there to guide the eyes.

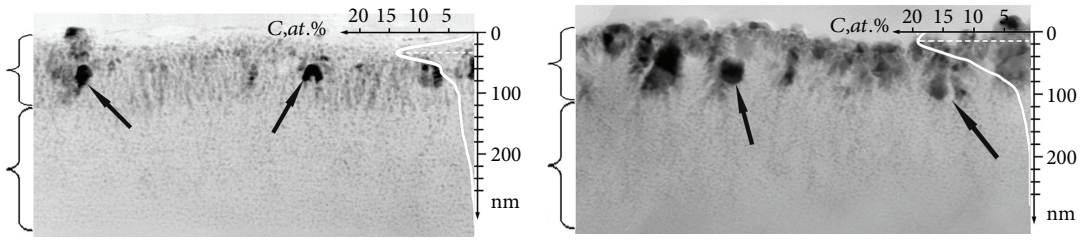

(a) (b)

FIGURE 3: XTEM images of SiO_2 (600 nm)/Si samples implanted with 200 keV Sn^+ to a fluence of 5×10^{16} cm^{-2} (a) and 1×10^{17} cm^{-2} (b) and annealed in an air atmosphere for 60 minutes at 900°C. In the right of each XTEM image, the depth distribution of Sn (given in at.%) is shown as detected by RBS. The braces are there to guide the eyes.

For the sample implanted to a fluence of 5×10^{16} cm^{-2} (Figure 1(a)), a band with small precipitates is observed at the depth of 40–180 nm. The average size of precipitates is ~5 nm. This sample is characterized by a Gaussian-like depth profile of Sn with a slight bend at the depth of 130 nm. This bend position coincides with a region depleted with Sn nanoclusters as seen in the corresponding TEM image into 120-130 nm from the surface (indicated by the arrow in Figure 1(a)).

For the sample implanted to a fluence of 1×10^{17} cm^{-2} (Figure 1(b)), a region of precipitates is located substantially closer to the surface and includes two layers differing in precipitate size. The first layer with a high density of large clusters (from 5 and up to 20 nm) is located in the depth range from the surface up to 100 nm. The second layer of small clusters (up to 2-3 nm) is observed at the depths of 130–180 nm. For the fluence of 1×10^{17} cm^{-2}, the depth of maximum impurity concentration shifts to the surface noticeably. This result is in a good agreement with the corresponding TEM image and can be caused by radiation-enhanced diffusion during high-fluence implantation. Though, even in the case of such high fluence, a comparison of the calculated Sn profile with the simulated one by SRIM (not shown here) reveals that there is no significant loss of tin in the sample.

The substantial broadening of the Sn concentration profile up to the depth of ~200 nm should be noted. Similar results of XTEM investigations of silica glasses implanted with a high fluence of Sn ions are reported in Ref. [11]. The authors of Ref. [11] have observed two layers of Sn precipitates in the as-implanted samples: a layer with large precipitates in the subsurface region and a layer with smaller clusters deeper in the sample. Precipitates (with an average size of ~9 nm) in the subsurface region (~100 nm) have been identified as metal β-Sn clusters by means of HRTEM image analysis and X-ray diffraction data. Taking this into account, we can assume that the dark contrast inclusions in the TEM

images of the as-implanted samples (Figures 1(a) and 1(b)) are precipitates of metallic β-Sn.

Heat treatment at 800°C (Figures 2(a) and 2(b)) results in a noticeable structural transformation of the implanted SiO_2 matrix as well as a substantial redistribution of the embedded impurity. For the fluence of 5×10^{16} cm^{-2} (Figure 2(a)), two layers with large Sn clusters (20-25 nm) are formed in the annealed sample at depths of 40 and 100 nm.

Simultaneously, the formation of two concentration peaks (8 and 12 at.% at the depths of ~40 and ~95 nm, respectively) in the impurity profile is observed in the same depth range. One can notice the dark particles of metal β-Sn on the sample surface. Evidently, these particles are formed due to impurity "squeezing" through the surface. For the fluence of 1×10^{17} cm^{-2} (Figure 2(b)), the thermal oxidation changes drastically the impurity depth distribution, the morphology of the subsurface region, and the distribution of nanoparticles. It is observed that a preferential impurity migration towards the surface results in the increase in Sn concentration to ~18-20 at.% within a thin subsurface layer of ~20 nm. The TEM image of this sample reveals that Sn accumulation in the subsurface zone leads to swelling and, accordingly, to a strong deformation of the subsurface region: the before-flat surface of the sample becomes irregular (wave-like) with depth differences up to 50 nm (Figure 2(b)). In addition, the formation of well-defined dendrites of large and coalesced nanoparticles of grey contrast is observed (shown by the arrows in the XTEM image of Figure 2(b)). Part of these dendrites includes dark contrast clusters surrounded with grey contrast shells. The dendrites exhibit an elongated shape, and they are oriented normally to the surface. The region of dendrites extends from the surface up to a depth of 100 nm. Beneath the dendrite region, smaller precipitates with a size of 2–4 nm are present up to a depth of 260 nm from the surface.

In order to explain the appearance of dendrites, let us discuss the possible structural rearrangements in the SiO_2 matrix with a high concentration of embedded Sn that occurs at high temperatures. The system SnO–SiO_2 was studied in Refs. [20, 21]. SnO was noted to be highly soluble (up to 70%) in the amorphous SiO_2 matrix. However, SnO is metastable and decomposes into a metallic phase (β-Sn) and SnO_2 upon heating above 550°C. The metastable silicate $SiSnO_3$ can also form. In turn, this compound decomposes at $T >$ 700°C with the formation of β-Sn, SnO_2, and SiO_2. SnO_2 has a very low solubility in SiO_2. For example, only 0.2–2.0 vol% SnO_2 can be dissolved in quartz [22]. The low solubility of SnO_2 in SiO_2 was explained by the different bond strengths of Sn and Si to O. Furthermore, tetravalent tin (Sn^{4+}) forms with O atoms, a 6-coordinate polyhedral structure, in contrast with SiO_4 groups in SiO_2 [22]. SnO_2 at a high concentration in SiO_2 can form its own random layered network of polyhedral units (based on the asymmetric building block $(SnO_4)^{6-}$), thereby destroying the three-dimensional tetrahedral structure of the SiO_2 network. Taking the above into account, we can conclude that in our experiments the existence of dendrites in the subsurface region is most probably related to the formation of the SnO_2 phase. It is worth adding that similar TEM images were reported for SiO_2 implanted with Sn ions in Ref. [11]. According to Ref. [11], a thin (~8 nm) dense SnO_2 layer was formed in the subsurface region of the implanted sample. In addition, SnO_2 nanoclusters were created all over the implanted SiO_2 layer. These clusters were visible in XTEM by Moire contrast and identified as SnO_2 nanocrystals by X-ray diffraction measurements.

An increase in the oxidation temperature to 900°C results in substantial changes of the depth impurity profile for the sample implanted to the fluence of 5×10^{16} cm^{-2} (Figure 3(a)). Tin concentration at the subsurface impurity peak at the depth of ~40 nm increases to 11 at.% while the second impurity peak at 100 nm transforms into a diffusion tail into the depth of the sample ranging up to 300 nm. Tin concentration in this region does not exceed 5 at.%. As can be seen from the corresponding TEM image, a structural rearrangement of the subsurface zone takes place. Instead of two layers with precipitates as shown in Figure 2(a), a dense layer of precipitates with embedded large dark particles is formed in the subsurface region (shown by the arrows in the XTEM image of Figure 3(a)). The thickness of this layer is ~120 nm. For the sample implanted to the fluence of 1×10^{17} cm^{-2} and annealed at 900°C, there is no noticeable change in the Sn concentration profile in comparison with that obtained after oxidation at 800°C (Figure 3(b)). The TEM image of that sample does not show any noticeable structural transformations, too. It is worth mentioning the interesting feature in the TEM images of the samples implanted to both fluences and heated at 900°C, namely, the existence of the uniform distribution of nanoclusters with a size of several nanometers at depths from 100 to 300 nm (Figures 3(a) and 3(b)). This depth region is depleted with impurity in comparison with the subsurface SiO_2 layer and is characterized with Sn concentration < 5 at.%. Probably, when the impurity concentration is low, Sn atom diffusion to the SiO_2/Si interface begins to prevail over Sn precipitation. That is why, small Sn-based clusters can be formed deeper in the SiO_2 layer than one expects from the analysis of the initial as-implanted Sn concentration profiles. A similar effect was reported in Ref. [3] devoted to the study of Sn precipitation in the SiO_2 matrix with relatively low concentration of embedded Sn atoms. The SiO_2 (180 nm)/Si samples were implanted with tin ions (200 keV, 1.5×10^{16} cm^{-2}) corresponding to the Gaussian-type Sn concentration-depth profile with peak concentrations ≈ 3 at.% formed at the depth of 90 nm in the SiO_2 matrix. According to the TEM data, Sn nanoclusters with the average size of 2.2 nm were formed in the SiO_2 layer after annealing at 900°C in vacuum. These precipitates were distributed uniformly in the volume of the SiO_2 matrix. The authors of Ref. [3] concluded that such distribution arises probably due to the absence of trapping centers, allowing the Sn diffusion from the original as-implanted Gaussian-type profile towards the surface and to the SiO_2/Si interface. As a consequence, the formation of large Sn clusters and SnO_x shells around them was not observed.

To study the phase composition of the annealed samples, "plan-view" TEM and electron microdiffraction investigations were carried out (Figure 4). Annealing of samples at 800°C results in the formation of precipitates with sizes ranging from 2 to 30 nm (Figure 4(a)). Besides, specific contrast

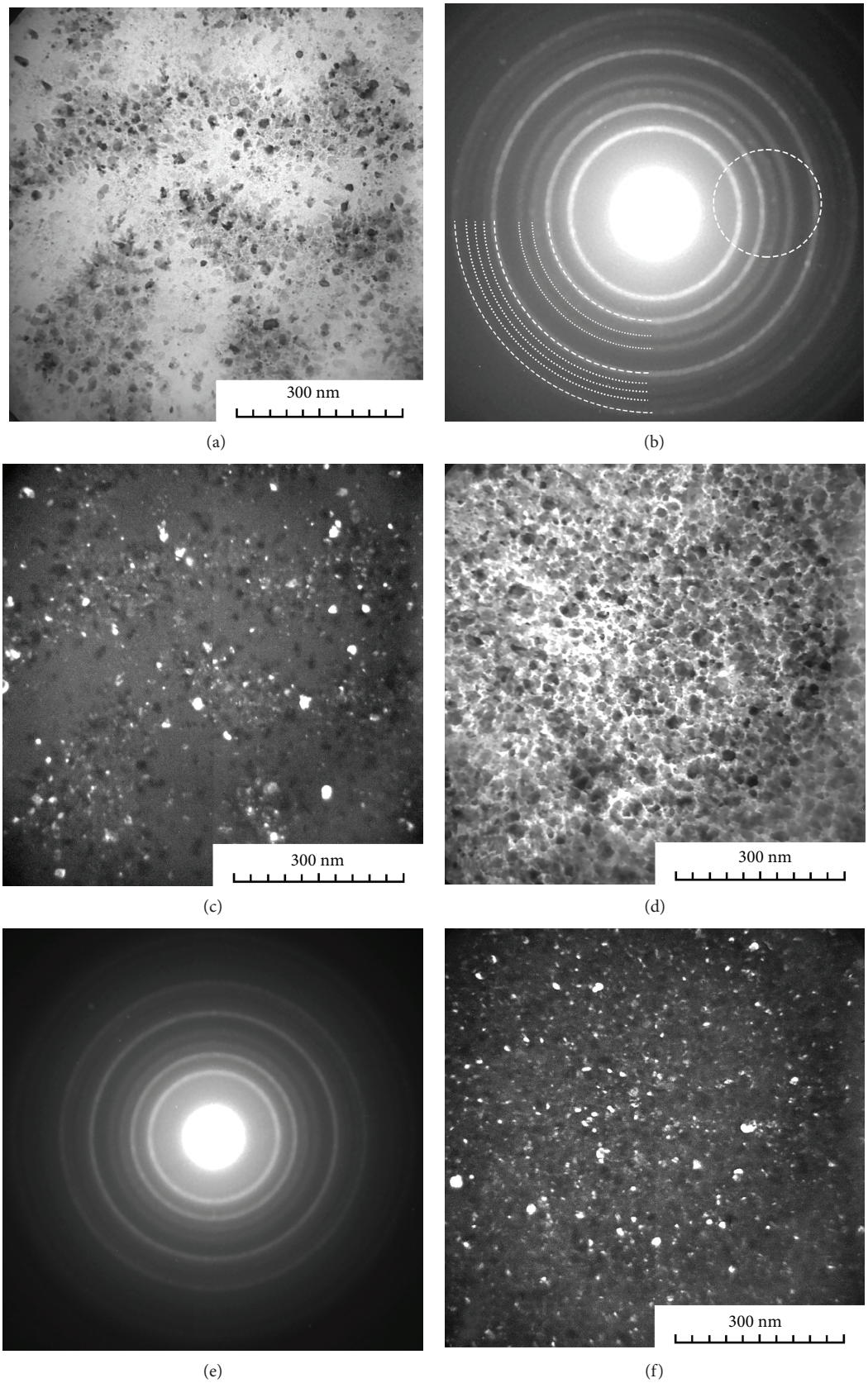

FIGURE 4: Bright-field (a, d) and dark-field TEM images (c, f) and electron diffraction patterns (b, e) of SiO_2 (600 nm)/Si samples implanted with 200 keV Sn^+ to a fluence of 1×10^{17} cm^{-2} and annealed at 800 (a, b, c) and 900°C (d, e, f).

(alternating curved light and dark stripes) is observed in the images. An annealing temperature increase (up to 900°C) results in the reduction of this contrast and cluster size increase (up to 50 nm) (Figure 4(d)). The crystal structure of the clusters is confirmed by the presence of narrow rings in diffraction patterns (Figures 4(b) and 4(e)) and their "light-up" on dark-field TEM micrographs (Figures 4(c) and 4(f)). These dark-field images were formed by the diffracted beams from the area shown in Figure 4(b). The values of interplanar spacing obtained from electron microdiffraction patterns were compared with the American X-ray ICDD PDF-2 database [23]. We do not exclude the formation of various tin phases (β-Sn, SnO, and $SiSnO_3$). However, the electron diffraction data have shown that the SnO_2 phase is the most probable (see Table 1).

3.2. Photoluminescence of "SiO_2+Sn-Based NC" Composites. Figure 5 depicts the PL spectra of the as-implanted samples and the spectra of implanted samples after annealing at 800°C and 900°C. The spectra of the as-implanted samples are characterized by a weak emission with maximum at the blue range (2.9 eV). The PL intensity significantly increases after thermal oxidation. A broad band of complicated shape dominates in all spectra. For the annealed samples, the narrowest and most intense band is located at the violet spectral range (~ 3.1 eV). There are other broad weak bands in the green-orange spectral range of 1.8–2.9 eV. It should be noted that the intensity of violet band with respect to the intensity of emission in the green-orange range increases with increasing ion fluence and annealing temperature.

Obviously, the complicated shape of the PL bands of Sn-implanted SiO_2/Si samples is due to a number of radiative centers. The nature of the narrow band in the violet spectral range (~3.1 eV) is the most intriguing one. It was mentioned above that the appearance of the strong PL at 3.18–2.97 eV is characteristic of bulk and nanostructured SnO_2 [11, 24–27]. The energy gap of bulk SnO_2 is 3.6 eV, and the Bohr radius of an exciton for SnO_2 amounts to 2.7 nm. This value (2.7 nm) is significantly lower than the size of the precipitates created in SiO_2 in our experiment. Hence, it is doubtful to expect the quantum confinement displayed in the PL spectra. At the same time, the energy of the exciting laser light (3.81 eV) used for PL recording in our experiment is quite enough to excite the band edge emission of SnO_2. Moreover, for the understanding of the observed PL spectra, one has to take the existence of a high concentration of oxygen vacancies in SnO_2 into account. This defect is the most common defect in nanostructured SnO_2 and in fact defines its electrical (n-type of conductivity) and optical properties. The oxygen vacancy in SnO_2 forms a donor defect level below the conduction band edge [11, 28]. Therefore, the origin of the emission at ~3.1 eV from SnO_2-based composites can be considered the edge band emission broadened due to excitons bounded to neutral donors [25] as well as a recombination of electrons located at the oxygen vacancies with a hole from the valence band [11, 24–27]. As noted in Ref. [29], a high oxygen vacancy concentration is a characteristic feature for Sn nanospheres coated with SnO_2 shells. Taking this into account, we can ascribe the observed intense PL peak at

Table 1: Comparison of the interplanar distances (d_{hkl}) of β-Sn and SnO_2 and the calculated ones from the electron diffraction pattern.

No. of diffraction rings	Calculated interplanar distances from electron diffraction data, Å	Interplanar distances and Miller indices, Å (hkl) [23]	
		β-Sn	SnO_2
1	3.318	—	3.349 (110)
2	2.632	2.608 (210)	2.643 (101)
3	2.306	—	2.308 (111)
4	2.086	2.062 (220)	2.118 (210)
5	1.755	1.730 (221)	1.764 (211)
6	1.673	1.659 (301)	1.675 (220)
7	1.577	1.590 (002)	1.579 (300)
8	1.488	1.484 (112)	1.482 (221)
9	1.410	—	1.415 (301)

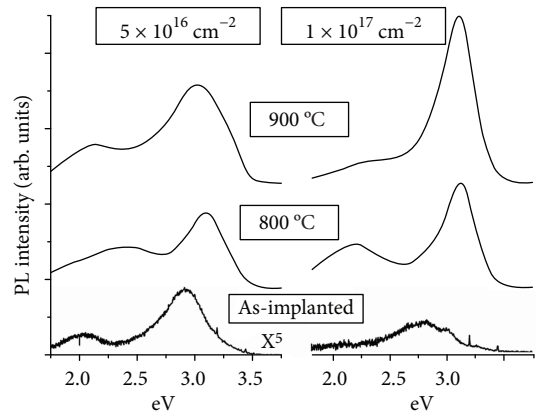

Figure 5: PL spectra of the implanted samples of SiO_2 (600 nm)/Si before and after annealing.

~3.1 eV to the formation of SnO_2 precipitates and/or SnO_2 shells surrounding Sn nanoclusters.

However, an alternative explanation of the origin of the "violet" band is possible. This feature can originate from molecular-like centers [1–3, 5, 30] corresponding to Sn-related oxygen-deficient centers (ODC) in the SiO_2 matrix itself. According to Ref. [5], the PL band at 3.15 eV in Sn-doped silica samples can be excited by light in the near ultraviolet region (like in our experiment) and caused by intercombination transition ($T_1 \rightarrow S_0$). Nevertheless, attribution of the violet band to Sn-ODC in the case of our samples is illegitimate. Firstly, it has been found that high-temperature annealing for an hour results in a significant violet PL increase. If the nature of such PL increase is related to twofold coordinated Sn atoms, we should suppose the increase in concentration of twofold coordinated Sn atoms dissolved in the silica matrix after annealing. However, in conditions of our experiment, it is unlikely. Secondly, the registered PLE spectrum at PL maximum (Figure 6) exhibits one band with maximum at 3.4 eV. It does not coincide with the maximum of excitation spectra at 3.7 eV in near UV and does not exhibit band in middle UV as observed in the PLE spectrum

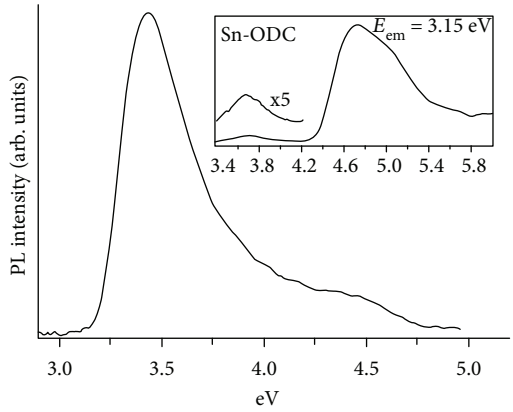

FIGURE 6: PLE spectrum of the SiO_2 (600 nm)/Si samples implanted with 200 keV Sn^+ to a fluence of 1×10^{17} cm^{-2} and annealed in an air atmosphere for 60 minutes at 900°C. The inset shows the PLE spectrum for the emission at 3.15 eV ($T_1 \rightarrow S_0$) attributed to twofold coordinated Sn atoms in SiO_2 from Ref. [5].

for violet band (3.15 eV) attributed to Sn-ODC [5] (inset in Figure 6). Thus, the violet band at 3.1 eV can be attributed to the SnO_2 phase (in the form of separate clusters or Sn cluster shells). It should be noted that the excitation band is at 3.4 eV (lower than the SnO_2 band edge, 3.6 eV) and its edge on the low-energy side is not steep enough. It is additionally proven that effective energy gap contraction is probably due to structural imperfection of synthesized nanocrystals.

There is a still open question asking which synthesized nanoclusters (large ones and dendrites near the surface or small regular nanoprecipitates in more deep regions of the SiO_2 film) play a crucial role in violet PL. In order to shed more light on this question, we have carried out an additional etching experiment for the sample implanted to the fluence of 1×10^{17} cm^{-2} and subsequently annealed at 900°C. The aim of this experiment was to remove a thin subsurface layer of nearly 50 nm. Figure 7 shows the PL spectra of the unetched sample and the sample with the upper layer being etched away. As can be seen from Figure 7, the etch procedure results in the decrease in intensity of violet band at 3.1 eV. Therefore, the large clusters formed in the subsurface layer with high Sn concentration (~20%) are more responsible for the emission in the violet spectral range. Simultaneously, one can see an increase in the intensity in the spectral range of 1.8–2.9 eV. Most probably, the weak and broad band in this spectral range originates from defects in both SnO_2 (Sn and O interstitials, dangling bonds, or oxygen vacancies) [5, 9, 24, 25, 27, 31] and SiO_2 matrix [24, 30, 32, 33] and also from the formation of the SnO_x phase [34]. It is noncontradictory, and the contribution of defects in the SiO_2 matrix and SnO_x phase in emission would be higher from the more deep layers due to lower concentration of Sn atoms and oxygen atoms diffused from air.

Interestingly, for both fluences, the ratio of the emission intensity in the range of 1.8–2.9 eV to the emission intensity at 3.1 eV decreases when increasing the oxidation temperature from 800°C to 900°C. It can be explained by improving

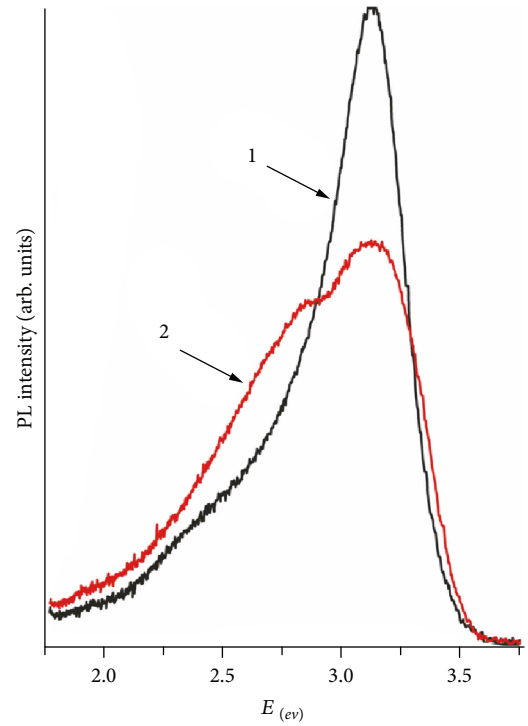

FIGURE 7: PL spectra of the SiO_2 samples implanted with Sn ion (1×10^{17} cm^{-2}) and annealed at 900°C before (1) and after (2) etching of the upper layer.

the crystallinity of the tin oxide nanoparticles and reducing the intrinsic defect concentration.

There is one peculiarity which additionally proves the formation of the SnO_2 phase. Earlier, we estimated that the etch velocity of SiO_2 layers thermally grown on Si substrates amounted to ≈18 nm/min [35]. Hence, one could expect that the thickness of the SiO_2 layer removed during 3 min etching should be about 50 nm, and it could be noticed via the film color change between the protected and unprotected regions of the etched sample. However, we have noticed the film color change only after additional fourfold repetition of the 3 min treatment in 4% HF (the etching total duration was 15 min). At the same time, it is known that SnO_2 films practically do not dissolve in HF solutions (see, for example, [36]). Hence, we can suggest the existence of the subsurface layer of the low-soluble SnO_2 phase also from the low etching rate.

4. Conclusions

The embedded impurity distribution, structural and light emission properties of "SiO_2+Sn-based NC" composites created via high-fluence tin ion implantation, and thermal oxidation in air were studied using RBS, XTEM, and PL. A strict correspondence of Sn concentration profiles and tin-based particle distribution in the SiO_2 layer has been found. Nanoclusters of β-Sn (diameter ranging from 2 to 10 nm) are formed in a 180 nm thick layer of the SiO_2 layer after ion implantation. Upon heat treatment, the diffusion of

embedded tin impurity to the surface and into the depth of the SiO_2 layer is observed. For the sample implanted to a fluence of 1×10^{17} cm^{-2} and heated at 800°C, the impurity accumulation in the subsurface zone leads to swelling and strong deformation: the originally flat surface of the sample becomes irregular (wave-like). The dendrites composed of large and coalesced nanoparticles of grey contrast are created in the subsurface region of the implanted SiO_2 matrix. The appearance of dendrites is most probably due to the formation of the SnO_2 phase. For the samples implanted to both fluences and heated at 900°C, beneath the layer of big dark particles surrounded by grey contrast shells, a uniform distribution of nanoclusters with a size of several nanometers at the depths from 100 to 300 nm is observed. This depth region is depleted with impurity in comparison with the subsurface SiO_2 layer (Sn concentration < 5 at.%). The formation of the SnO_2 phase in annealed films was proven by diffraction patterns.

The PL spectra of the as-implanted samples are characterized by a weak emission with maximum at the blue range (2.9 eV). The PL intensity significantly increases after the thermal oxidation. The narrowest and most intense PL band has a maximum at ~3.1 eV. Its intensity increases with increasing fluence and annealing temperature. We conclude that this emission can be assigned to the formation of the SnO_2 phase (in the form of separate clusters or shells of Sn clusters) in the subsurface region of the implanted SiO_2 matrix.

Data Availability

The data used to support the findings of this study are available from the corresponding author upon request.

Conflicts of Interest

The authors declare that they have no conflicts of interest.

Acknowledgments

This work was partly supported by the Belarusian Republican Foundation for Fundamental Research (Grant F17KIG-005).

References

[1] L. Rebohle, J. von Borany, H. Fröb, and W. Skorupa, "Blue photo- and electroluminescence of silicon dioxide layers ion-implanted with group IV elements," *Applied Physics B: Lasers and Optics*, vol. 71, no. 2, pp. 131–151, 2000.

[2] S. Spiga, R. Mantovan, M. Fanciulli et al., "Local structure of Sn implanted in thinSiO2films," *Physical Review B*, vol. 68, no. 20, article 205419, 2003.

[3] J. M. J. Lopes, F. C. Zawislak, P. F. P. Fichtner, F. C. Lovey, and A. M. Condo, "Effect of annealing atmosphere on the structure and luminescence of Sn-implanted SiO2 layers," *Applied Physics Letters*, vol. 86, no. 2, article 23101, 2005.

[4] J. M. J. Lopes, F. Kremer, P. F. P. Fichtner, and F. C. Zawislak, "Correlation between structural evolution and photoluminescence of Sn nanoclusters in SiO_2 layers," *Nuclear Instruments and Methods in Physics Research Section B: Beam Interactions with Materials and Atoms*, vol. 242, no. 1-2, pp. 157–160, 2006.

[5] L. Skuja, "Isoelectronic series of twofold coordinated Si, Ge, and Sn atoms in glassy SiO2: a luminescence study," *Journal of Non-Crystalline Solids*, vol. 149, no. 1-2, pp. 77–95, 1992.

[6] H.-J. Fitting, "How to make silica luminescent?," *Journal of Luminescence*, vol. 129, no. 12, pp. 1488–1492, 2009.

[7] Y. Wang, J. He, P. Barua et al., "Ultraviolet photoluminescence in Gd-doped silica and phosphosilicate fibers," *APL Photonics*, vol. 2, no. 4, 2017.

[8] O. V. Laguta, H. E. Hamzaoui, M. Bouazaoui, V. B. Arion, and I. M. Razdobreev, "On the nature of photoluminescence in bismuth-doped silica glass," *Scientific Reports*, vol. 7, no. 1, p. 3178, 2017.

[9] X. Zhang, R. Chen, P. Wang et al., "A soft chemistry-based route to enhanced photoluminescence of terbium ions and tin oxide nanocrystals codoped silica thin films," *Applied Surface Science*, vol. 452, pp. 96–101, 2018.

[10] X. Xiang, X. T. Zu, S. Zhu et al., "Photoluminescence of SnO_2 nanoparticles embedded in Al2O3," *Journal of Physics D: Applied Physics*, vol. 41, no. 22, article 225102, 2008.

[11] M. A. Tagliente, V. Bello, G. Pellegrini, G. Mattei, P. Mazzoldi, and M. Massaro, "SnO2 nanoparticles embedded in silica by ion implantation followed by thermal oxidation," *Journal of Applied Physics*, vol. 106, no. 10, article 104304, 2009.

[12] D. A. Zatsepin, A. F. Zatsepin, D. W. Boukhvalov, E. Z. Kurmaev, and N. V. Gavrilov, "Sn-loss effect in a Sn-implanted a -SiO 2 host-matrix after thermal annealing: a combined XPS, PL, and DFT study," *Applied Surface Science*, vol. 367, pp. 320–326, 2016.

[13] C. Gu, J. Huang, N. Ni, M. Li, and J. Liu, "Detection of DNA hybridization based on SnO_2 nanomaterial enhanced fluorescence," *Journal of Physics D: Applied Physics*, vol. 41, no. 17, article 175103, 2008.

[14] P. K. Kuiri, H. P. Lenka, J. Ghatak, G. Sahu, B. Joseph, and D. P. Mahapatra, "Formation and growth of SnO_2 nanoparticles in silica glass by Sn implantation and annealing," *Journal of Applied Physics*, vol. 102, no. 2, article 24315, 2007.

[15] T. W. Kim, D. U. Lee, and Y. S. Yoon, "Microstructural, electrical, and optical properties of SnO2 nanocrystalline thin films grown on InP (100) substrates for applications as gas sensor devices," *Journal of Applied Physics*, vol. 88, no. 6, pp. 3759–3761, 2000.

[16] J. Jeong, S.-P. Choi, C. I. Chang et al., "Photoluminescence properties of SnO_2 thin films grown by thermal CVD," *Solid State Communications*, vol. 127, no. 9-10, pp. 595–597, 2003.

[17] L. Z. Liu, X. L. Wu, J. Q. Xu, T. H. Li, J. C. Shen, and P. K. Chu, "Oxygen-vacancy and depth-dependent violet double-peak photoluminescence from ultrathin cuboid SnO_2 nanocrystals," *Applied Physics Letters*, vol. 100, no. 12, article 121903, 2012.

[18] J. Henrie, S. Kellis, S. M. Schultz, and A. Hawkins, "Electronic color charts for dielectric films on silicon," *Optics Express*, vol. 12, no. 7, p. 1464, 2004.

[19] S. M. Sze, *Physics of Semiconductor Devices*, J. Wiley & Sons, Ann Arbor, Michigan, 1981.

[20] M. M. Karim and D. Holland, "Physical properties of glasses in the system SnO-SiO_2," *Physics and Chemistry of Glasses*, vol. 36, p. 206, 1995.

[21] J. F. Bent, A. C. Hannon, D. Holland, and M. M. A. Karim, "The structure of tin silicate glasses," *Journal of Non-Crystalline Solids*, vol. 232-234, pp. 300–308, 1998.

[22] M. B. Volf, *Chemical Approach to Glass*, Elsevier, Oxford, UK, 1984.

[23] ICDD PDF-2 (Database), *American Society for Testing and Materials (ASTM)*, Soorya Kabekkodu, Ed., International Centre for Diffraction Data, Newtown Square, PA, USA, 1997.

[24] T.-Y. Wei, S.-Y. Lu, and Y.-C. Chang, "Rich photoluminescence emission of SnO_2–SiO_2 composite aerogels prepared with a co-fed precursor sol–gel process," *Journal of the Chinese Institute of Chemical Engineers*, vol. 38, no. 5-6, pp. 477–481, 2007.

[25] R. Chen, G. Z. Xing, J. Gao, Z. Zhang, T. Wu, and H. D. Sun, "Characteristics of ultraviolet photoluminescence from high quality tin oxide nanowires," *Applied Physics Letters*, vol. 95, no. 6, article 61908, 2009.

[26] L. C. Nehru, V. Swaminathan, and C. Sanjeeviraja, "Photoluminescence studies on nanocrystalline tin oxide powder for optoelectronic devices," *American Journal of Materials Science*, vol. 2, no. 2, pp. 6–10, 2012.

[27] A. R. Babar, S. S. Shinde, A. V. Moholkar, C. H. Bhosale, J. H. Kim, and K. Y. Rajpure, "Physical properties of sprayed antimony doped tin oxide thin films: the role of thickness," *Journal of Semiconductors*, vol. 32, no. 5, article 53001, 2011.

[28] S.-S. Chang and D. K. Park, "Novel Sn powder preparation by spark processing and luminescence properties," *Materials Science and Engineering B*, vol. 95, no. 1, pp. 55–60, 2002.

[29] S. Li, X. Zhong, Y. Song et al., "Controlled hybridization of Sn–SnO_2 nanoparticles via simple-programmed microfluidic processes for tunable ultraviolet and blue emissions," *Journal of Materials Chemistry C*, vol. 2, no. 36, pp. 7687–7694, 2014.

[30] A. Cannizzo, S. Agnello, M. Cannas, N. Chiodini, M. Leone, and A. Paleari, "Temperature dependence of luminescence decay in Sn-doped silica," *Journal of Non-Crystalline Solids*, vol. 351, no. 21-23, pp. 1937–1940, 2005.

[31] N. F. Santos, J. Rodrigues, T. Holz et al., "Luminescence studies on $SnO_2$and SnO_2:Eu nanocrystals grown by laser assisted flow deposition," *Physical Chemistry Chemical Physics*, vol. 17, no. 20, pp. 13512–13519, 2015.

[32] L.-S. Liao, X.-M. Bao, N.-S. Li, X.-Q. Zheng, and N.-B. Min, "Blue-, green-, and red-light emission from Si+-implanted thermal SiO2 films on crystalline silicon," *Journal of Luminescence*, vol. 68, no. 2-4, pp. 199–204, 1996.

[33] R. Tohmon, Y. Shimogaichi, H. Mizuno, Y. Ohki, K. Nagasawa, and Y. Hama, "2.7-eV luminescence in as-manufactured high-purity silica glass," *Physical Review Letters*, vol. 62, no. 12, pp. 1388–1391, 1989.

[34] H. H. An, S. J. Lee, S. H. Baek et al., "Effect of plasma etching on photoluminescence of SnO_x/Sn nanoparticles deposited on DOPC lipid membrane," *Journal of Colloid and Interface Science*, vol. 368, no. 1, pp. 257–262, 2012.

[35] L. A. Vlasukova, F. F. Komarov, V. N. Yuvchenko et al., "Threshold and criterion for ion track etching in SiO_2 layers grown on Si," *Vacuum*, vol. 105, pp. 107–110, 2014.

[36] C. E. Morosanu, *Thin Films by Chemical Vapour Deposition*, Elsevier, Oxford, 1990.